PAPER

Check for updates

Soft electrodes in water desalination: application to multi-valent ions

G. R. Iglesias, [ID] [a] S. Ahualli, [ID] [a] M. M. Fernández,[b]
M. L. Jiménez [ID] [a] and A. V. Delgado [ID] *[a]

The capacitive deionization (CDI) method, in which the capacitance of the electrical double layers is used for removing ions from aqueous solutions, can be more efficient if some procedures are devised to help the bare electrode double layers in adsorbing ions. One of these methods is based on the use of ion-selective membranes (membrane–CDI or MCDI). An alternative has been proposed, in which the electrodes are coated with a polyelectrolyte layer, also of suitable polarity. The method has been called soft electrode CDI or SECDI. In this work, we examine how it can be applied to a mixed solution containing divalent and monovalent cations, specifically, sodium and magnesium, identifying to what extent each of them is removed from the solution. A model is presented in which the polyelectrolyte is assumed to coat the macro-pore walls, and hence the mouths of the micropores connected to them. The results of the model, corroborated by experimental determinations of SECDI in mixed solutions of NaCl and $MgCl_2$, demonstrate that magnesium, even if in tiny amounts, dominates the deionization with soft electrodes, as it is more abundant in the polyelectrolyte layer than sodium.

Water impact

The huge electrical capacitance of electrical double layers has brought about explosive interest in the field of water purification and constitutes the basis of capacitive deionization (CDI). Using polyelectrolyte-coated (soft) electrodes, the CDI performance increases significantly. This idea is applied to the realistic case of mixed solutions containing suitable proportions of monovalent and divalent cations.

1. Introduction

The need for potable water does not always run parallel to access to either natural water resources or to drinking water production plants.[1] The main methods for large-scale production of potable water from seas, lakes or rivers involve large installations, high power, significant investment, and so on. This refers to reverse osmosis, accounting for about 65% of the total,[2] multi-stage flash distillation (around 20%), electrodialysis, ion-exchange, and others, used to a lesser extent, or as pre-treatments for other methods.[3] More recently, interest is growing in the possible implementation of forward osmosis,[4,5] membrane distillation,[6,7] pervaporation,[8] or solar desalination techniques.[9–14] The latter can be adapted as easily implementable methods for water desalination, accessible to medium or small-size communities often far from industrial areas, and hence they constitute an excellent tool for life quality enhancement.[14–18]

One technique fulfilling such requirements and recently highly developed is capacitive deionization or CDI.[19–29] In this and related methods, it is precisely the characteristics of the solid/salt solution interface on the nanometer scale that are exploited. If a pair of high surface-area conductive electrodes (typically activated carbon) are connected to the terminals of a dc power source and placed in contact with a saline solution, counterions are adsorbed on the corresponding electrodes (co-ions are expelled at the same time, but to a lesser extent), leaving a less concentrated solution, that can in principle reach the admissible drinking-water concentration (roughly 250 mg L^{-1} NaCl, see for instance the World Health Organization guideline[30]). For electrode regeneration, the electrodes are either short-circuited or their polarity is reversed so that ions are released again into the bulk and discharged as brackish water.

In recent works, an improvement has been suggested consisting of placing ion exchange membranes on the porous electrodes, a procedure called membrane capacitive deionization or MCDI.[31–36] The selectivity of the membranes enhances adsorption of the corresponding counterions while preventing desorption of the co-ions. In principle, for each electron

[a] *Department of Applied Physics, Faculty of Science, Campus Fuentenueva, University of Granada, 18071 Granada, Spain. E-mail: adelgado@ugr.es*
[b] *Department of Fluidic and Energy Science, Central America University, San Salvador, El Salvador*

This journal is © The Royal Society of Chemistry 2019

Environ. Sci.: Water Res. Technol., 2019, **5**, 873–883 | 873

transferred in MCDI between the electrodes, one monovalent salt molecule is removed from the bulk bringing about an efficiency close to 1. The regeneration step is also improved with this method. In ref. 37, we have proposed a variation of the technique in which instead of using separate ion exchange membranes, it is the electrodes themselves that behave as ion exchangers. This is achieved by coating the activated carbon particles forming the electrodes with a layer of polyelectrolyte, cationic or anionic correspondingly. Because of the similarity to the process of producing so-called soft particles in colloid science,[38–40] this configuration has been denominated as soft-electrode capacitive deionization (SECDI).[37,41,42] It must be mentioned that polyelectrolytes are not the only materials used for coating.[43] Apart from a resin shell used by Lee et al.[44] for increasing the carbon hydrophilicity, ion-selective layers are mostly used nowadays.[45] As an example, Kim et al.[46] used PVA and polysulfone for improving CDI, and Kim and Choi[47] demonstrated an increase of the efficiency from 0.67 to 0.85 by applying a cation exchange layer (cross-linked PVA-sulfosuccinic acid) to one of the electrodes.

Most experiments and theoretical modeling on CDI, MCDI and SECDI have dealt with simple NaCl solutions. However, contributions must be cited regarding fluoride removal from fluoride–chloride solutions,[48] and elaboration of a sequence of electrosorption specificities of both cations and anions,[49] based on hydrated radii and valencies.[50,51]

In the case of soft electrodes, the role of solution composition in desalination and the possible sorption preferences through the polyelectrolyte layers with different sizes and valencies have never been investigated. However, the topic is as important here as it is in either CDI or MCDI, because natural solutions to be desalinated come from the ocean or from lakes and they typically have a complex combination of dissolved ions. The objective of this paper is hence to carry out an investigation of the possible selectivity in removing the most abundant cations in sea water, namely Na^+ and Mg^{2+}, by SECDI. A model will be elaborated on the kinetics of each cation adsorption and the results will be compared with experimental data on their amounts in solution during the adsorption and desorption steps from soft electrodes.

2. Theoretical background

2.1. Fundamentals

In a typical CDI cell, a pair of activated carbon electrodes is placed in contact with an ionic solution. In the left part of Fig. 1, a schematic representation is shown of the hierarchical structure of the SE-CDI half-cell corresponding to one of the electrodes represented by a set of channels, the macropores (in the micrometer size range), which are the actual pathways for the ions from or towards the micropores, typically of nanometer size. The electrical double layers (EDLs) on the walls of the latter are the reservoirs where the ions are stored, providing the huge capacitance characteristic of the system. In this model, it is assumed that the polyelectrolyte molecules coat the walls of the macropores, to which many micropores can be connected. For the sake of EDL calculations, the polyelectrolyte is assumed to be located at the mouth of the micropore, determining the ionic concentration in the entrance and therefore the flow of ions going in or out of the micropore.

The model is used to predict the ionic concentration at the exit of the cell, based on the knowledge of the entrance concentration and the applied voltage or current. Consequently,[52,53] the channel is divided into a number of subcells $i = 1, \ldots, N$, as shown in Fig. 1, in each of which the ionic concentration is uniform but time dependent; the solutions involved in the CDI processes are to be imagined
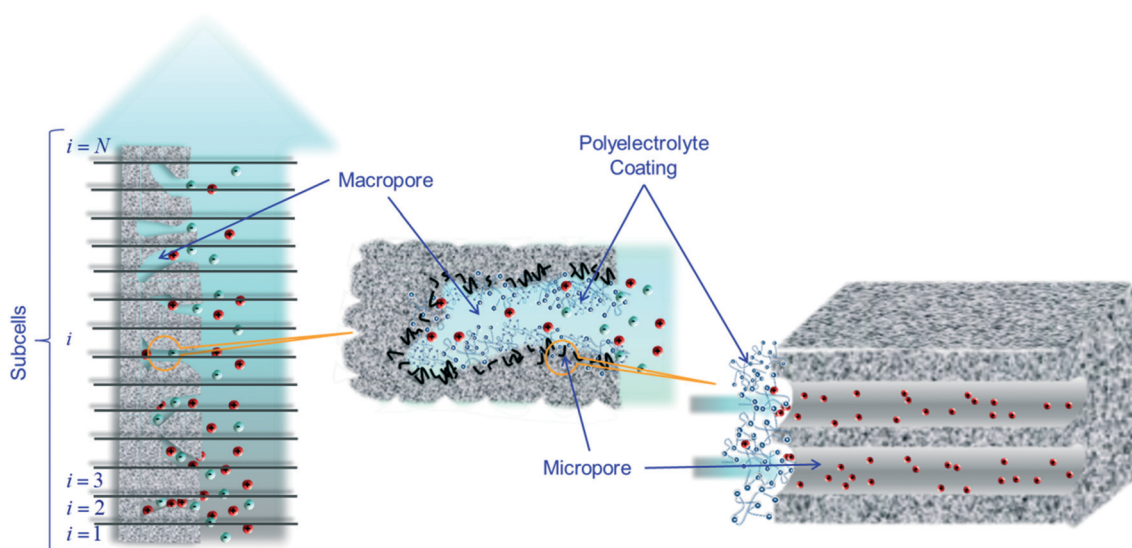

Fig. 1 Schematics of the assumed hierarchical structures of the SE-CDI half-cell. From left to right: The macropores are identified on the carbon wall; the walls of the macropores are coated with the polyelectrolyte molecules; many micropores are connected to each macropore; the polyelectrolyte is assumed to be located at the mouth of the micropore.

flowing in the upward direction in such a way that for subcell $i = 1$, the concentration of ionic species j, $c^*_{j,1}$, is higher than that for subcell 2, $c^*_{j,2}$, because of ion accumulation in the EDLs of the micropores connected to the macropores in that subcell. The exit concentration will correspond to that at the last compartment, $i = N$. The differences between two subsequent cells correspond to the migration of ions to micropores. Hence, in each of them, a continuity equation for the concentrations $c^*_{j,i}$ of each ionic species j at macropores can be established:

$$\left(L_{sp} + 2L_e p_M\right)\frac{dc^*_{j,i}}{dt} = -J^j_{i,M\rightarrow m} + \frac{\phi_v}{A_{sub}}\left(c^*_{j,i-1} - c^*_{j,i}\right) \quad (1)$$

where

• L_{sp} is the spacer thickness, *i.e.*, the average distance between the opposing electrodes.

• L_e is the electrode thickness.

• p_M is the fraction of pore volume corresponding to macropores.

• $J^j_{i,M\rightarrow m}$ stands for the flow of ion species j from the macropore to the micropore in subcell i.

• ϕ_v is the pumping flow rate.

• A_{sub} is the projected area of each electrode.

Eqn (1) expresses that the number of moles of type j ions per unit volume of subcell i changes with time because ions move from the macropores to the micropores (disappearing from the subcell if $J^j_{i,M\rightarrow m}$ is positive), or because they are pumped to or from neighboring cells (the ions are pumped in the subcell at a rate of $c^*_{j,i-1}$ (mol m^{-3}) $\times \phi_v$ (m^3 s^{-1}) and they leave from it at $c^*_{j,i} \times \phi_v$). The flow from macro- to micro-pores results in charge accumulation; for example, in the cathode, there will be an accumulation of sodium and magnesium ions due to the flow towards the micropores, while chloride ions leave them:

$$L_e\frac{d}{dt}\left(p_m\rho_{m,i}\right) = F\left[J^{Na}_{i,M\rightarrow m} - J^{Cl}_{i,M\rightarrow m} + 2J^{Mg}_{i,M\rightarrow m}\right] \quad (2)$$

where F is the Faraday constant, p_m is the micropore porosity fraction, and $\rho_{m,i}$ indicates the volume charge density in the micropores at subcell i. This equation expresses that the micropores acquire charge thanks to the fluxes of ions from the macropores. But the accumulation of ions cannot proceed without limits; neglecting the diffusive transport, the fluxes are controlled by the potential difference between micro- and macropores, $\Delta\Psi_{tr,i}$, in turn given by the applied potential difference between the electrodes, V_{ext}, and the EDL potential, including both Stern and diffuse components:

$$J^j_{i,M\rightarrow m} = -z_j D_j c^{SE}_{j,i} L_{eff}^{-1}\Delta\Psi_{tr,i}$$
$$\Delta\Psi_{tr,i} = V_{ext}/2 - \left(\Delta\Psi_{St,i} + \Delta\Psi_{d,i}\right) \quad (3)$$

The modified Donnan (mD) model is often considered as valid to solve the EDL structure in micropores, as the strong EDL overlap from opposite walls suggests that both the electric potential and the ionic concentration are roughly constant inside the micropores. According to this model, the Stern and diffuse potentials are given by:

$$\Delta\Psi_{St,i} = -\frac{\rho_{m,i}}{C_{St}k_B T}$$
$$\rho_{m,i} = \sum_j z_j F c^*_{j,i}\exp\left(-z_j e\Delta\Psi_{d,i}/k_B T\right) \quad (4)$$

where C_{St} is the Stern capacitance per unit volume, and both potentials are made dimensionless by the thermal voltage $k_B T/e$.

2.2. Consideration of the polyelectrolyte layers

Note that in eqn (3), the soft polyelectrolyte layer determines the concentration of each species at the micropore entrance, hence the factor $c^{SE}_{j,i}$, which should not be confused with $C^*_{j,i}$. In fact, a given ionic concentration at the macropore will determine another one at the soft layer. This fact leads us to consider the potential and ionic profiles in the double layer surrounding the polyelectrolyte (Fig. 2), by solving the Poisson–Boltzmann equation for a polyelectrolyte charge density equal to ρ_{pol} subject to suitable boundary conditions, as detailed in ref. 41 and 54. From the solution of these equations, it is possible to find the concentration of each ion j in subcell i, inside the polyelectrolyte layer. These data will be used as inputs for the time evolution problem through eqn (3).[37] The equations are as follows:
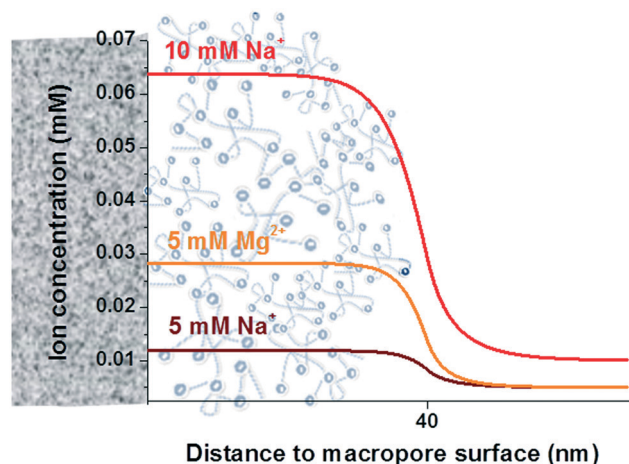

Fig. 2 Counterion concentration profiles close to a negative macropore surface, both inside the region occupied by the polyelectrolyte and outside it, for pure NaCl 10 mM solution, and for a mixed solution of 5 mM NaCl + 5 mM MgCl$_2$. Charge density of the polyelectrolyte: -3×10^6 C m^{-3}.

This journal is © The Royal Society of Chemistry 2019

Environ. Sci.: Water Res. Technol., 2019, **5**, 873–883 | 875

$$\nabla^2 \Psi(r) = -\frac{F}{\varepsilon_m \varepsilon_0} \left[c_{Na,i}(r) + 2c_{Mg,i}(r) - c_{Cl,i}(r) \right] - \frac{1}{\varepsilon_m \varepsilon_0} \rho_{pol} \; (\text{inside the layer})$$

$$\nabla^2 \Psi(r) = -\frac{F}{\varepsilon_m \varepsilon_0} \left[c_{Na,i}(r) + 2c_{Mg,i}(r) - c_{Cl,i}(r) \right] (\text{outside the layer})$$

$$c_{j,i}(r) = c_{j,i}^* \exp\left(-\frac{z_i e \Psi}{k_B T} \right) (\text{everywhere})$$

(5)

2.3. Predictions

Fig. 2 shows the concentration profiles in the anionic polyelectrolyte layer for the three ions considered, and for either a pure 10 mM NaCl or a mixed NaCl (5 mM) and MgCl$_2$ (5 mM) solution in contact with the polyelectrolyte-coated macropore surface. Note that in all cases, the counterion concentrations are almost constant in the region occupied by the polymer, provided that the thickness of this layer is much larger than the Debye length, as it is usually the case.

The electrostatic interactions (we are not considering here the effect of ion size) between the charged chains and the ions provoke that the divalent ions are more concentrated than the monovalent ones if both are equally concentrated in the bulk. Thus the presence of magnesium renders the concentration of sodium almost negligible. Because the concentration in the region occupied by the polymer coating (the mouth of micropores) determines the ionic flows from macropore to micropore, these results are very important in understanding the role of soft electrodes; the flux of counterions will be favored and that of co-ions will be (almost) blocked and, what is more important in this work, the presence of divalent ions will affect the adsorption of the monovalent ions in solution.

With this kind of result, it is possible to find the ionic profiles in the spacer channel, $c_{j,i}^*$, for each subcell i as a function of time assuming that a solution at a fixed concentration is continuously pumped along the channel. As an example, Fig. 3 displays such profiles for the simplest case of a 20 mM NaCl solution and the parameters indicated. Note that the concentration at the uppermost subcell corresponds to the exit concentration, and hence is a measure of the evolution of desalination.

From Fig. 3, it is possible to understand the operation mode of a desalination cell according to the theoretical model. At the input, the cell receives at any time a solution at a given concentration to be desalinated. As the solution flows through the cell, it is purified, decreasing its concentration, as can be observed for the upper subcells.

It is also of interest to consider the concentration profiles in the case of pure MgCl$_2$, and, more importantly, of mixtures of equal concentrations of NaCl and MgCl$_2$. Fig. 4a demonstrates that they are qualitatively similar for both counterions, although the double valence of Mg^{2+} screens the surface charge with lower concentration than in the case of sodium ions. Furthermore, the slightly faster diffusion of magnesium results in maximum deionization in a shorter time. In the case of mixtures (Fig. 4b), the stronger electrostatic interac-

tions between magnesium ions and the cathode retain larger amounts of the former in the pores and the soft layer, thus resulting in lower deionization than in sodium salt. For these systems, the kinetics remains basically unaltered, although the competition between both ions leads to very significant alterations of the time profiles; the presence of magnesium reduces the adsorption of sodium, and the amount of the latter in the exit solution is always higher than that of magnesium. The explanation of this behavior is shown in Fig. 2; the presence of the soft layer favors the flow of Mg^{2+} with respect to Na$^+$ in the case of the mixed solution, and hence the micropores will be filled preferably with divalent ions. This is the fast ion and is transported in a shorter time towards the polyelectrolyte shell, leaving sodium behind.

3. Materials and methods

3.1. Materials

The carbon used for building the electrodes is denominated as SR-51, and was manufactured by MAST Carbon International, Ltd. Its total pore volume amounts to 0.67 cm^3 g^{-1}, with a specific surface area of 959 m^2 g^{-1}. The polyelectrolytes employed are PSS (anionic, MW 200 kg mol^{-1}) and PDADMAC (cationic, 100 kg mol^{-1}), both from Sigma-Aldrich (USA).

3.2. Methods

The carbon films were produced following standard methods;[37] a suspension was first prepared containing 3 g of
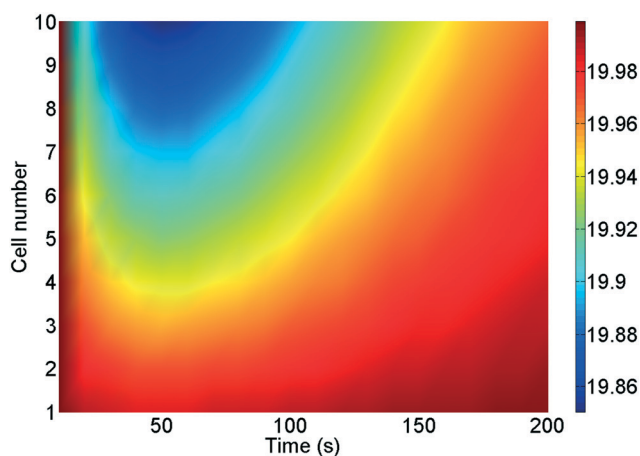

Fig. 3 Na$^+$ concentration profile (20 mM input concentration) as a function of time for different subcells in the spacer channel. "Cell number" indicates the number of subcell ($i = 1, \ldots, N$) where 1 corresponds to the inlet of the cell and 10 to its exit. The color code indicates mM concentration.
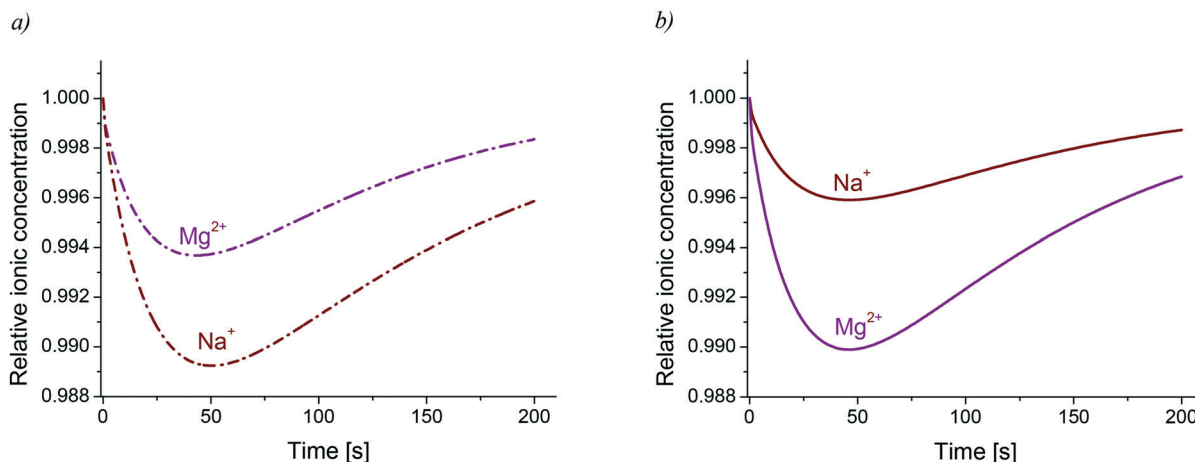
a)

b)

Fig. 4 Sodium and magnesium concentrations at the exit of the cell as a function of time, for solutions containing (a) 10 mM NaCl or MgCl$_2$, and (b) mixtures of equal volumes of both solutions (5 mM NaCl + 5 mM MgCl$_2$).
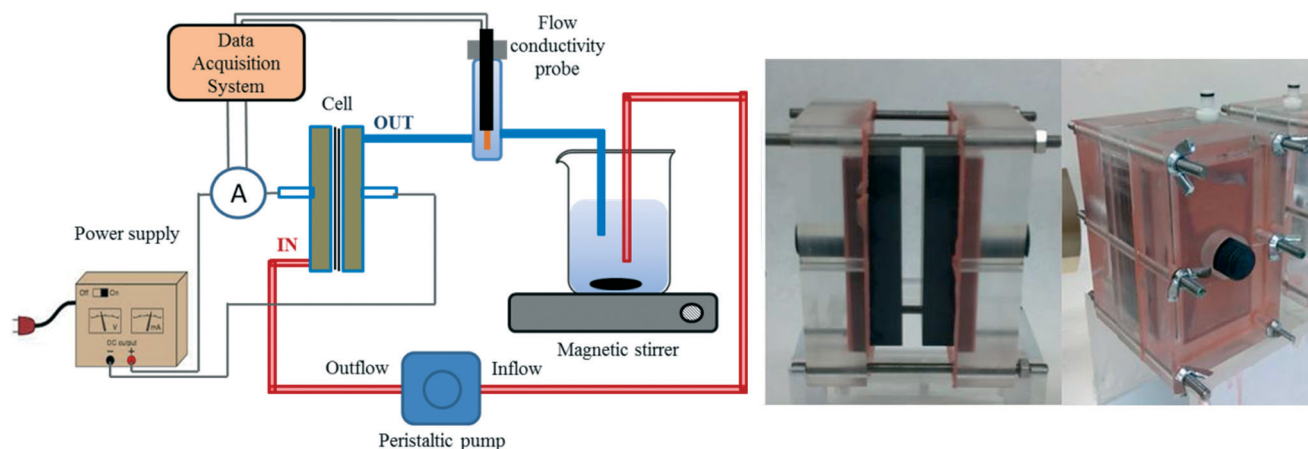

Fig. 5 The layout of the desalination procedure and the deionization cell used in the present work.

activated carbon and 10 g of a 33 g L^{-1} solution of poly(vinylidene-fluoride) (PVDF, manufactured by Arkema, USA) in 1-methyl 2-pyrrolidone (Sigma Aldrich) as the binder. This was heated to 60 °C and sonicated for one hour in a thermostatic bath. The resulting slurry was spread on the graphite collector (rectangular, 10 × 5 cm^2 dimensions, Fig. 5) leaving a 0.2 mm layer, and this was dried at 60 °C overnight. The resulting layers were converted into "soft" electrodes by the simple procedure of keeping them in 500 mL of a 100 mM (on a monomer basis) solution of the corresponding polyelectrolyte for 24 h under constant stirring. Stability of the coating was indirectly demonstrated by the reproducibility of the deionization cycles after about 100 repetitions. More direct evidence was obtained by measuring the total organic content (TOC) of a solution after 100 passes through the inter-electrode space. A Skalar Formacs TOC/TN analyzer (the Netherlands) was used for this purpose. This must be considered in comparison with the estimated amount of polyelectrolyte adsorption on the carbon electrodes. Using the results published by Matsui *et al.*[55] regarding PSS adsorption on activated carbon, we can estimate that for the solution in contact with the electrodes (containing

8 g PDADMAC), the adsorbed amount is 204 mg PSS per g of carbon. In our case, the mass of carbon is 0.34 g per electrode. This means that the adsorbed polymer amount will be 69 mg. According to the analysis, the amount of polymer desorbed is 0.169 mg from each electrode, representing just 0.2% loss of polyelectrolyte. We assume that the behavior is symmetric, although we have no explicit data on PDADMAC. It can be expected that this cationic polymer will be even more strongly adsorbed on the negative bare carbon surface.

In a typical example of operation, the incoming solution is pumped from the bottom to the upper part of the cell with open-circuit electrodes for 30 minutes. After this time, an adsorption step begins by connecting the electrodes to an external power source (constant potential, 900 mV) while the conductivity and current are recorded with a 520413-Sensor Cassy data acquisition unit (Leybold, Germany). A 529670-conductivity and temperature probe, also from Leybold, is connected just at the exit of the cell recording in this way the solution conductivity during CDI cycles. When the current goes to zero and the conductivity remains constant, the power source is reversed, the desorption cycle starts, and the

process is continued until a stable response is obtained. The cycles are repeated several times but, for the sake of simplicity, only one of them will be presented in the Results section. It must be mentioned, though, that the deionization behaviour was found repeatable for over one hundred cycles, confirming the stable attachment of the polyelectrolytes to the electrodes.

In the case of single salts, it is usual and straightforward to obtain the salt concentration from the conductivity *vs.* time curves (as given in Fig. 6). When mixed electrolytes are subject to deionization, the raw conductivity data cannot provide enough information in order to identify which ions are actually present in solution. This can be achieved by measuring the concentration of each of the cations, Na^+ or Mg^{2+}, separating a few millilitres from the exit of the cell at different times during the cycle. These samples were analyzed by means of ion chromatography (940 Professional IC Vario, Metrohm, Switzerland) for anionic and cationic analysis, with a precision of 1 $\mu g\ L^{-1}$. For comparison purposes, all concen-

tration data (including those of single salt solutions) were obtained using the latter method.

4. Results and discussion

4.1. Pure NaCl and MgCl₂ solutions

Fig. 6 shows a typical series of desalination/regeneration cycles corresponding in this case to pure 10 mM NaCl and 10 mM $MgCl_2$. The current peaks coincide with those of conductivity changes, and the whole processes of adsorption and desorption take roughly five minutes each. The first part of the cycle is associated with the adsorption step, where the ions move to the electrodes decreasing the solution conductivity. However, as fresh solution is being continuously pumped and the EDLs of the micropores are full, the ion migration stops when the potential decay in the EDL (including the Stern layer) compensates for V_{ext} (eqn 3) bringing about a decline of the current to zero, and a return of the conductivity to the value of the feed solution. The second part is the
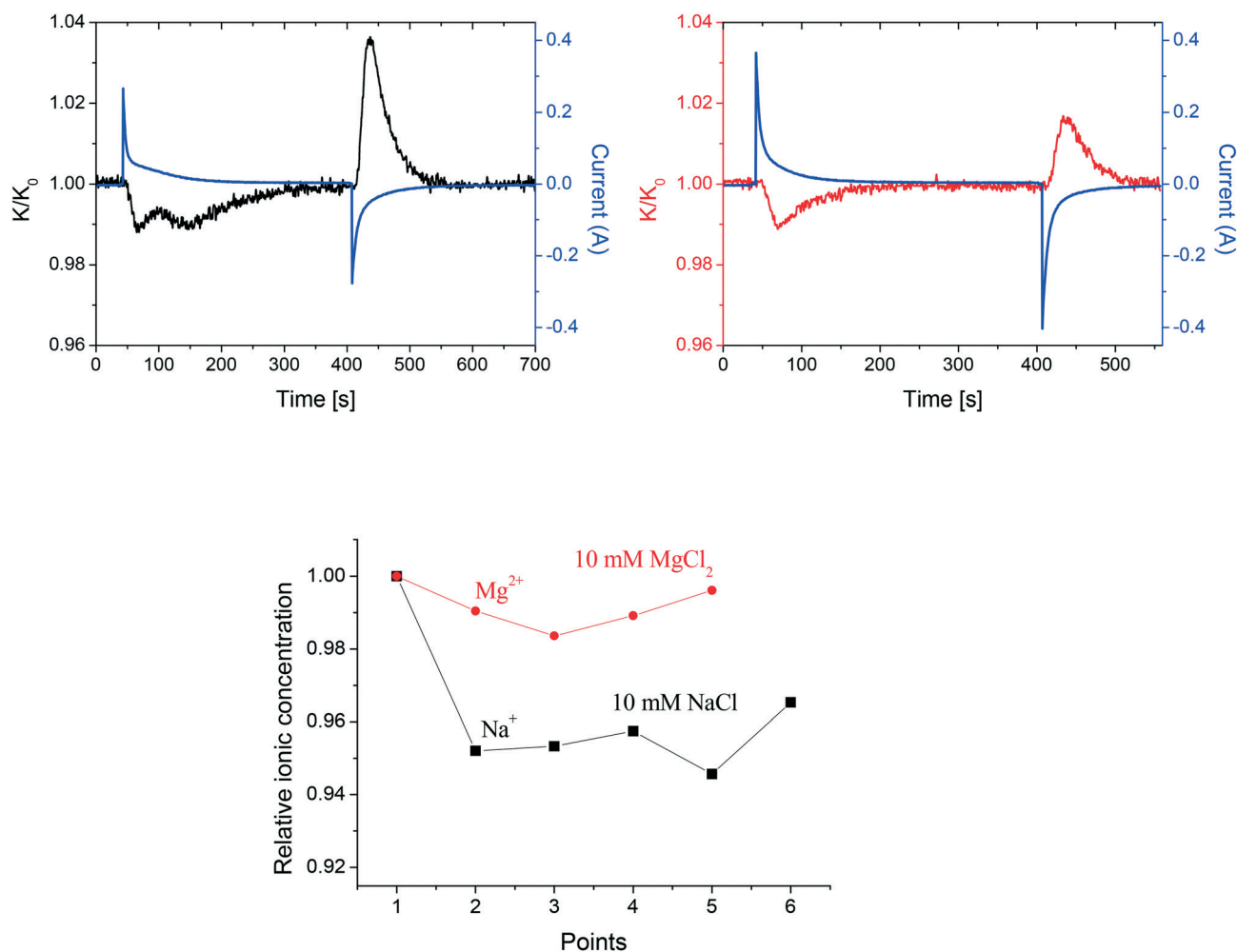

Fig. 6 Typical evolution of the conductivity (left axis) and current (right axis) in the CDI experiment. Applied voltage: 900 mV. The desorption cycle is performed under reverse conditions (opposite voltage polarity). Incoming solutions: 10 mM NaCl (upper left panel) and 10 mM MgCl₂ (upper right). Bottom: Relative concentrations of magnesium and sodium ions obtained from ion chromatography, for 10 mM NaCl and 10 mM MgCl₂. The points correspond to those in Fig. 8 and 9 (data taken every 40 s).

desorption step. Here, an opposite voltage depletes the micropore giving rise to a current in the opposite direction. A very important point is that ions leaving one electrode will not move to the opposite one because the polyelectrolyte layer blocks them. For this reason, as in the case of membrane-CDI, and in contrast to bare-carbon CDI, a single conductivity peak is observed during each polarity of the applied voltage.[32,37]

As a quantitative measure of the deionization efficiency is achieved, the salt adsorption capacity, SAC, is used in the field. This quantity is defined as:[43,56]

$$SAC = \frac{M_{salt}}{m_{elec}} \int_0^{t_{ads}} (c_{out} - c_{in}) \phi_v \, dt \qquad (6)$$

where M_{salt} is the molecular weight of the salt, m_{elec} is the mass of both electrodes, t_{ads} is the duration of the adsorption step of the cycle, and c_{out} (c_{in}) is the concentration of the outgoing (ingoing) solution. Since we have determined by ion chromatography (IC) the concentrations of each type of ion at different stages of the adsorption curves, SAC was obtained in all cases by calculating the concentration in solution after B-spline interpolation of the IC results.

Another key parameter for evaluating the CDI performance is charge efficiency, ε, which measures how many ion charges are adsorbed for each electron transferred from one electrode to the other. This can be calculated as:

$$\varepsilon = zF \frac{\int_0^{t_{ads}} (c_{out} - c_{in}) \phi_v \, dt}{\int_0^{t_{ads}} I(t) \, dt} \qquad (7)$$

F is the Faraday constant, z is the valence of the ionic species, and $I(t)$ is the current measured as a function of time.

4.2. Desalination of mixed solutions

For the purpose of comparing the experimental results with those obtained from the theory, it is necessary to measure the amount of the single ionic species during the adsorption step. Solutions with different Na^+/Mg^{2+} molar ratios (25%, 50%, and 75%) were prepared in order to explore the reciprocal influence of each of them on their storage in the EDL. The results corresponding to 50% mixed solutions, 5 mM NaCl and 5 mM $MgCl_2$, are exemplified by the data in Fig. 7; the conductivity as a function of time shows an intermediate trend between those of the pure solutions (comparison of the characteristic times of the cycles shown in Fig. 6 and 7). The differences between $MgCl_2$ and NaCl solutions are mainly related to the dynamics of ion adsorption, which was also predicted by the theoretical model (Fig. 4a). The relative ionic concentrations of sodium and magnesium ions for pure solutions of NaCl and $MgCl_2$ change when the solutions are mixed at the same ratio; while magnesium ions are less adsorbed than sodium when pure 10 mM solutions are used, in the case of mixed solutions, the same behavior of theoretical predictions (Fig. 4) is observed; the divalent ions are preferably adsorbed compared to the monovalent ones.

The concentrations of the respective cations at different stages of the deionization cycles are represented in Fig. 8 and 9. As observed, the shape of the conductivity trends (left panels of Fig. 8 and 9) approaches those obtained for pure sodium chloride or magnesium chloride (Fig. 6), according to the amount of the most abundant cation. The experimental data obtained from ion chromatography (right panels of Fig. 8 and 9) show that each ionic species follows a time evolution trend parallel to that of conductivity. There is almost no time lag between them, in good agreement with the theoretical predictions (Fig. 4b).

On the other hand, we can observe that Mg^{2+} dominates even in the case that sodium chloride is 75% in solution (Fig. 9), that is, the divalent ions seem to hinder sodium transport, a behavior that agrees very well with the predictions of
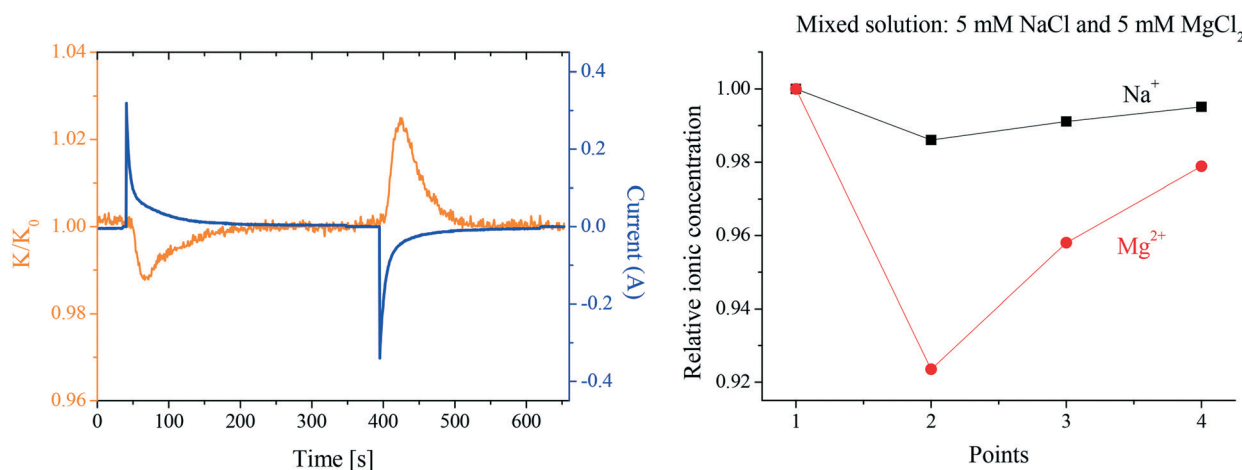

Fig. 7 Same as Fig. 6, but for mixed NaCl and $MgCl_2$ solutions, 5 mM each.
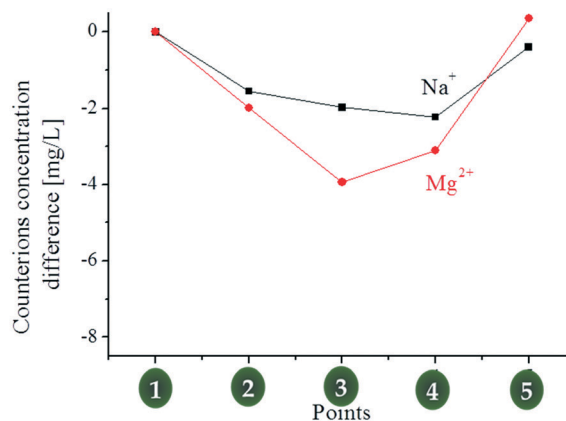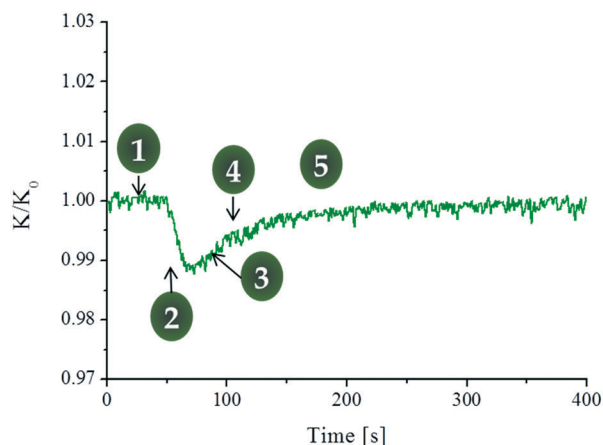
Fig. 8 Conductivity (relative to its initial value) *vs.* time and respective Na$^+$ and Mg^{2+} concentrations. Initial solution: 2.5 mM NaCl + 7.5 mM MgCl$_2$.
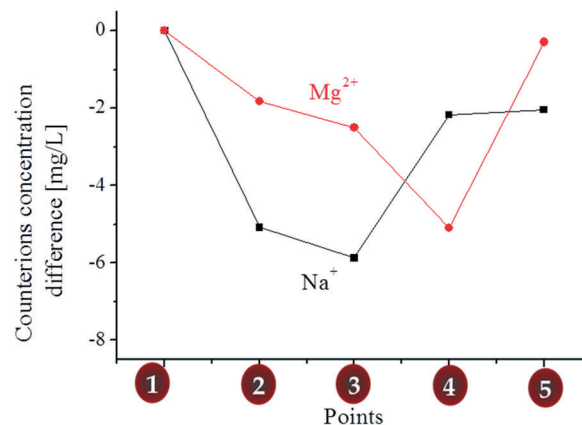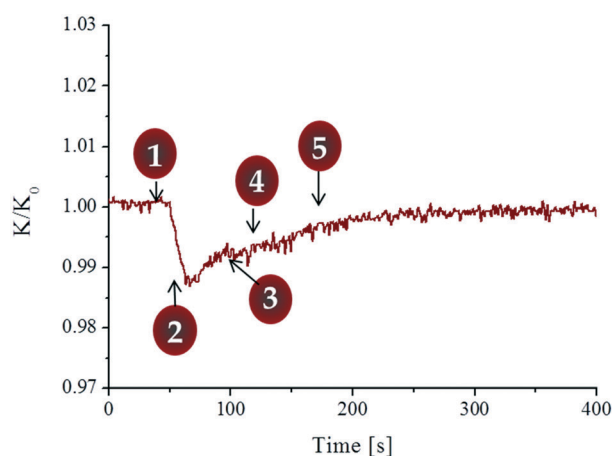

Fig. 9 Same as Fig. 8, but for solutions initially containing: 7.5 mM NaCl + 2.5 mM MgCl$_2$.

the model detailed above. If we look back at Fig. 2, it is possible to recognize that the concentration of divalent ions at the entrance of micropores is higher than that of the monovalent ones, and hence it can be said that they are preferably transported towards the EDL, leaving the solution.

The calculations of SAC and ε for both the single salt and the mixed solutions are included in Table 1. Note that the presence of the divalent Mg^{2+} ion reduces both quantities, as the higher charge can neutralize the interfacial charge with a smaller amount of counterions, thus decreasing the SAC. Regarding the reduction in efficiency, the larger size of these ions hinders their approach to the pore wall, leaving them at a comparatively large distance from it, less strongly attached to the wall. The same arguments apply to the mixed solutions; Mg^{2+} makes it difficult for Na$^+$ to get adsorbed.[57,58] As a result, both SAC and ε decrease. In this case, our model calculations (Fig. 2 and 4) already predicted the selectivity of the polyelectrolyte layer for the divalent cations over the monovalent ones.

According to Table 1, the charge efficiency reaches values close to 0.7 for solutions predominantly containing NaCl, and 0.4–0.5 for those with higher MgCl$_2$ concentration. We may wonder whether, as in the case of MCDI, the presence of

the polyelectrolyte layers avoid the occurrence of Faradaic reactions. The data published by Tang *et al.*[59] show that the efficiency increases from CDI to MCDI, mainly due to co-ion expulsion and partly to the avoidance of Faradaic processes. In our case, such a study was reported in a previous work,[37] where we found that at 0.9 V and 20 mM NaCl, the charge efficiency increased from 0.65 to 0.99, confirming the improvement associated with the coating. Based on these data, we can conclude that, with 900 mV used for charging, the role of Faradaic reactions appears to be negligible also for soft electrodes. Confirmation of this fact was obtained by pH determination of input (pH 6.2) and exit solutions (pH 5.2) during the deionization stage.

Table 1 Specific adsorption capacity and charge efficiency for the solutions indicated

Solution	SAC (mg g^{-1})	ε
NaCl 10 mM	3.4	0.66
MgCl$_2$ 10 mM	1.14	0.40
NaCl 5 mM + MgCl$_2$ 5 mM	0.18 (Na$^+$) + 0.96 (Mg^{2+})	0.53
NaCl 2.5 mM + MgCl$_2$ 7.5 mM	0.39 (Na$^+$) + 0.59 (Mg^{2+})	0.43
NaCl 7.5 mM + MgCl$_2$ 2.5 mM	0.93 (Na$^+$) + 0.62 (Mg^{2+})	0.72

880 | *Environ. Sci.: Water Res. Technol.*, 2019, **5**, 873–883

This journal is © The Royal Society of Chemistry 2019

5. Conclusions

A theory for soft electrodes as deionizing tools in CDI has been developed in this paper to consider ionic solutions containing ions of arbitrary valence. In particular, we have focused on the effect of the presence of magnesium in solution. We find that the latter ion is transported faster than sodium, and most importantly, when present in the solution, dominates to a large extent in the deionization process, leaving sodium almost unaltered in solution. The larger abundance of divalent counterions in the soft polyelectrolyte layer accounts for this fact. Experimental results confirm these predictions: the deionization kinetics is faster in solutions containing magnesium, and even tiny amounts of this cation hinder the removal of sodium to a large extent.

Conflicts of interest

There are no conflicts to declare.

Acknowledgements

References

1 M. A. Shannon, P. W. Bohn, M. Elimelech, J. G. Georgiadis, B. J. Marinas and A. M. Mayes, Science and technology for water purification in the coming decades, *Nature*, 2008, **452**(7185), 301–310.

2 S. Burn, M. Hoang, D. Zarzo, F. Olewniak, E. Campos, B. Bolto and O. Barron, Desalination techniques - A review of the opportunities for desalination in agriculture, *Desalination*, 2015, **364**, 2–16.

3 S. Jamaly, N. N. Darwish, I. Ahmed and S. W. Hasan, A short review on reverse osmosis pretreatment technologies, *Desalination*, 2014, **354**, 30–38.

4 L. A. Hoover, W. A. Phillip, A. Tiraferri, N. Y. Yip and M. Elimelech, Forward with Osmosis: Emerging Applications for Greater Sustainability, *Environ. Sci. Technol.*, 2011, **45**(23), 9824–9830.

5 D. L. Shaffer, J. R. Werber, H. Jaramillo, S. H. Lin and M. Elimelech, Forward osmosis: Where are we now?, *Desalination*, 2015, **356**, 271–284.

6 B. L. Pangarkar, M. G. Sane, S. B. Parjane and M. Guddad, Status of membrane distillation for water and wastewater treatment-A review, *Desalin. Water Treat.*, 2014, **52**(28–30), 5199–5218.

7 B. L. Pangarkar, S. K. Deshmukh, V. S. Sapkal and R. S. Sapkal, Review of membrane distillation process for water purification, *Desalin. Water Treat.*, 2016, **57**(7), 2959–2981.

8 Q. Z. Wang, N. Li, B. Bolto, M. Hoang and Z. L. Xie, Desalination by pervaporation: A review, *Desalination*, 2016, **387**, 46–60.

9 S. Gorjian and B. Ghobadian, Solar desalination: A sustainable solution to water crisis in Iran, *Renewable Sustainable Energy Rev.*, 2015, **48**, 571–584.

10 J. H. Reiff and W. Alhalabi, Solar-thermal powered desalination: Its significant challenges and potential, *Renewable Sustainable Energy Rev.*, 2015, **48**, 152–165.

11 H. Sharon and K. S. Reddy, A review of solar energy driven desalination technologies, *Renewable Sustainable Energy Rev.*, 2015, **41**, 1080–1118.

12 M. Edalatpour, K. Aryana, A. Kianifar, G. N. Tiwari, O. Mahian and S. Wongwises, Solar stills: A review of the latest developments in numerical simulations, *Sol. Energy*, 2016, **135**, 897–922.

13 A. K. Kaviti, A. Yadav and A. Shukla, Inclined solar still designs: A review, *Renewable Sustainable Energy Rev.*, 2016, **54**, 429–451.

14 M. Chandrashekara and A. Yadav, Water desalination system using solar heat: A review, *Renewable Sustainable Energy Rev.*, 2017, **67**, 1308–1330.

15 L. Elasaad, A. Bilton, L. Kelley, O. Duayhe and S. Dubowsky, Field evaluation of a community scale solar powered water purification technology: A case study of a remote Mexican community application, *Desalination*, 2015, **375**, 71–80.

16 L. Kelley, H. Elasaad and S. Dubowsky, Autonomous operation and maintenance of small-scale PVRO systems for remote communities, *Desalin. Water Treat.*, 2015, **55**(10), 2843–2855.

17 Y. Aroussy, M. Nachtane, D. Saifaoui, M. Tarfaoui, Y. Farah and M. Abid, Using renewable energy for seawater desalination and electricity production in the site OCP Morocco, *J. Sci. Arts*, 2016(4), 395–406.

18 N. Heck, A. Paytan, D. C. Potts and B. Haddad, Predictors of local support for a seawater desalination plant in a small coastal community, *Environ. Sci. Policy*, 2016, **66**, 101–111.

19 J. B. Lee, K. K. Park, H. M. Eum and C. W. Lee, Desalination of a thermal power plant wastewater by membrane capacitive deionization, *Desalination*, 2006, **196**(1–3), 125–134.

20 Y. Oren, Capacitive deionization (CDI) for desalination and water treatment - past, present and future (a review), *Desalination*, 2008, **228**(1–3), 10–29.

21 M. A. Anderson, A. L. Cudero and J. Palma, Capacitive deionization as an electrochemical means of saving energy and delivering clean water. Comparison to present desalination practices: Will it compete?, *Electrochim. Acta*, 2010, **55**(12), 3845–3856.

22 H. B. Li, L. D. Zou, L. K. Pan and Z. Sun, Novel Graphene-Like Electrodes for Capacitive Deionization, *Environ. Sci. Technol.*, 2010, **44**(22), 8692–8697.

23 H. B. Li, L. Zou, L. K. Pan and Z. Sun, Using graphene nanoflakes as electrodes to remove ferric ions by capacitive deionization, *Sep. Purif. Technol.*, 2010, **75**(1), 8–14.

This journal is © The Royal Society of Chemistry 2019

Environ. Sci.: Water Res. Technol., 2019, **5**, 873–883 | 881

24 S. Porada, L. Weinstein, R. Dash, A. van der Wal, M. Bryjak, Y. Gogotsi and P. M. Biesheuvel, Water Desalination Using Capacitive Deionization with Microporous Carbon Electrodes, *ACS Appl. Mater. Interfaces*, 2012, **4**(3), 1194–1199.

25 R. Zhao, P. M. Biesheuvel and A. van der Wal, Energy consumption and constant current operation in membrane capacitive deionization, *Energy Environ. Sci.*, 2012, **5**(11), 9520–9527.

26 Y. A. C. Jande and W. S. Kim, Desalination using capacitive deionization at constant current, *Desalination*, 2013, **329**, 29–34.

27 S. Porada, L. Borchardt, M. Oschatz, M. Bryjak, J. S. Atchison, K. J. Keesman, S. Kaskel, P. M. Biesheuvel and V. Presser, Direct prediction of the desalination performance of porous carbon electrodes for capacitive deionization, *Energy Environ. Sci.*, 2013, **6**(12), 3700–3712.

28 S. Porada, R. Zhao, A. van der Wal, V. Presser and P. M. Biesheuvel, Review on the science and technology of water desalination by capacitive deionization, *Prog. Mater. Sci.*, 2013, **58**(8), 1388–1442.

29 P. M. Biesheuvel, S. Porada, A. van der Wal and V. Presser, *Carbon Nanomaterials*, ed. Y. Gogotsi and V. Presser, CRC Press, Boca Raton, USA, 2014, pp. 419–461.

30 *Guidelines for Drinking-water Quality*, Recommendations, WHO, Geneva, 2006.

31 P. M. Biesheuvel and A. van der Wal, Membrane capacitive deionization, *J. Membr. Sci.*, 2010, **346**(2), 256–262.

32 P. M. Biesheuvel, R. Zhao, S. Porada and A. van der Wal, Theory of membrane capacitive deionization including the effect of the electrode pore space, *J. Colloid Interface Sci.*, 2011, **360**(1), 239–248.

33 J. Y. Lee, S. J. Seo, S. H. Yun and S. H. Moon, Preparation of ion exchanger layered electrodes for advanced membrane capacitive deionization (MCDI), *Water Res.*, 2011, **45**(17), 5375–5380.

34 S. I. Jeon, H. R. Park, J. G. Yeo, S. Yang, C. H. Cho, M. H. Han and D. K. Kim, Desalination via a new membrane capacitive deionization process utilizing flow-electrodes, *Energy Environ. Sci.*, 2013, **6**(5), 1471–1475.

35 C. Yan, Y. W. Kanaththage, R. Short, C. T. Gibson and L. D. Zou, Graphene/Polyaniline nanocomposite as electrode material for membrane capacitive deionization, *Desalination*, 2014, **344**, 274–279.

36 J. S. Kim, C. S. Kim, H. S. Shin and J. W. Rhim, Application of synthesized anion and cation exchange polymers to membrane capacitive deionization (MCDI), *Macromol. Res.*, 2015, **23**(4), 360–366.

37 S. Ahualli, G. R. Iglesias, M. M. Fernandez, M. L. Jimenez and A. V. Delgado, Use of Soft Electrodes in Capacitive Deionization of Solutions, *Environ. Sci. Technol.*, 2017, **51**(9), 5326–5333.

38 S. Ahualli, M. Luisa Jimenez, F. Carrique and A. V. Delgado, AC Electrokinetics of Concentrated Suspensions of Soft Particles, *Langmuir*, 2009, **25**(4), 1986–1997.

39 M. L. Jimenez, A. V. Delgado, S. Ahualli, M. Hoffmann, A. Witteman and M. Ballauff, Giant permittivity and dynamic mobility observed for spherical polyelectrolyte brushes, *Soft Matter*, 2011, **7**(8), 3758–3762.

40 H. Ohshima, Electrokinetic phenomena of soft particles, *Curr. Opin. Colloid Interface Sci.*, 2013, **18**(2), 73–82.

41 S. Ahualli, M. L. Jimenez, M. M. Fernandez, G. Iglesias, D. Brogioli and A. V. Delgado, Polyelectrolyte-coated carbons used in the generation of blue energy from salinity differences, *Phys. Chem. Chem. Phys.*, 2014, **16**(46), 25241–25246.

42 M. M. Fernandez, R. M. Wagterveld, S. Ahualli, F. Liu, A. V. Delgado and H. V. M. Hamelers, Polyelectrolyte-versus membrane-coated electrodes for energy production by capmix salinity exchange methods, *J. Power Sources*, 2016, **302**, 387–393.

43 S. Ahualli, G. R. Iglesias and A. V. Delgado, Principles and theoretical models of CDI: Experimental approaches in Charge and Energy Storage, in *Electrical Double Layers*, ed. S. Ahualli and A. V. Delgado, Academic Press-Elsevier, London, UK, 2018, pp. 169–192.

44 J. B. Lee, K. K. Park, S. W. Yoon, P. Y. Park, K. I. Park and C. W. Lee, Desalination performance of a carbon-based composite electrode, *Desalination*, 2009, **237**(1–3), 155–161.

45 Y. Liu, L. K. Pan, X. T. Xu, T. Lu, Z. Sun and D. H. C. Chua, Enhanced desalination efficiency in modified membrane capacitive deionization by introducing ion-exchange polymers in carbon nanotubes electrodes, *Electrochim. Acta*, 2014, **130**, 619–624.

46 J. S. Kim, Y. S. Jeon and J. W. Rhim, Application of poly(vinyl alcohol) and polysulfone based ionic exchange polymers to membrane capacitive deionization for the removal of mono- and divalent salts, *Sep. Purif. Technol.*, 2016, **157**, 45–52.

47 Y. J. Kim and J. H. Choi, Improvement of desalination efficiency in capacitive deionization using a carbon electrode coated with an ion-exchange polymer, *Water Res.*, 2010, **44**(3), 990–996.

48 W. Tang, P. Kovalsky, B. Cao, D. He and T. D. Waite, Fluoride Removal from Brackish Groundwaters by Constant Current Capacitive Deionization (CDI), *Environ. Sci. Technol.*, 2016, **50**(19), 10570–10579.

49 M. Mossad and L. D. Zou, A study of the capacitive deionisation performance under various operational conditions, *J. Hazard. Mater.*, 2012, **213**, 491–497.

50 C.-H. Hou and C.-Y. Huang, A comparative study of electrosorption selectivity of ions by activated carbon electrodes in capacitive deionization, *Desalination*, 2013, **314**, 124–129.

51 Y. Li, C. Zhang, Y. Jiang, T.-J. Wang and H. Wang, Effects of the hydration ratio on the electrosorption selectivity of ions during capacitive deionization, *Desalination*, 2016, **399**, 171–177.

52 P. M. Biesheuvel, B. van Limpt and A. van der Wal, Dynamic Adsorption/Desorption Process Model for Capacitive Deionization, *J. Phys. Chem. C*, 2009, **113**(14), 5636–5640.

53 W. Tang, P. Kovalsky, D. He and T. D. Waite, Fluoride and nitrate removal from brackish groundwaters by batch-mode capacitive deionization, *Water Res.*, 2015, **84**, 342–349.

882 | *Environ. Sci.: Water Res. Technol.*, 2019, **5**, 873–883

This journal is © The Royal Society of Chemistry 2019

54 H. Ohshima, Donnan potential and surface potential of a spherical soft particle in an electrolyte solution, *J. Colloid Interface Sci.*, 2008, **323**(1), 92–97.

55 Y. Matsui, N. Ando, T. Yoshida, R. Kurotobi, T. Matsushita and K. Ohno, Modeling high adsorption capacity and kinetics of organic macromolecules on super-powdered activated carbon, *Water Res.*, 2011, **45**, 1720–1728.

56 M. E. Suss, S. Porada, X. Sun, P. M. Biesheuvel, J. Yoon and V. Presser, Water desalination via capacitive deionization: what is it and what can we expect from it?, *Energy Environ. Sci.*, 2015, **8**(8), 2296–2319.

57 M. L. Jiménez, S. Ahualli, P. Arenas-Guerrero, M. M. Fernández, G. Iglesias and A. V. Delgado, Multiionic effects on the capacitance of porous electrodes, *Phys. Chem. Chem. Phys.*, 2018, **20**, 5012–5020.

58 M. L. Jiménez, S. Ahualli and M. M. Fernández, The Electrical Double Layer as a Capacitor. Evaluation of Capacitance in different Solutions: Effect of Ion Concentrations, Sizes, and Valencies, in *Charge and Energy Storage in Electrical Double Layers*, ed. S. Ahualli and A. V. Delgado, Academic Press-Elsevier, London, UK, 2018, pp. 39–62.

59 W. W. Tang, D. He, C. Y. Zhang, P. Kovalsky and T. D. Waite, Comparison of Faradaic reactions in capacitive deionization (CDI) and membrane capacitive deionization (MCDI) water treatment processes, *Water Res.*, 2017, **120**, 229–237.

This journal is © The Royal Society of Chemistry 2019

Environ. Sci.: Water Res. Technol., 2019, **5**, 873–883 | 883